DOI https: //doi. org/10.1007/s11595-019-2014-1

Effects of N Doping on the Microstructures and Optical Properties of TiO_2

XU Tao, WANG Mo, WANG Tong

(College of Civil Engineering, Nanjing Forestry University, Nanjing 210037, China)

Abstract: TiO_2 nanopowders with different nitrogen (N) dopant concentrations were first synthesized by sol-gel method. XRD, TEM, HRTEM, XPS, UV−vis DRS were used to characterize the effects of N doping on the microstructures and optical properties of TiO_2. The results indicated that the prepared TiO_2 only contained anatase phase with a slight distortion, and the N doping improved the dispersity of TiO_2. The N doping leaded to more defects in TiO_2, capturing the charge carriers and inhibiting the combination of electrons and holes. Also, the N−doped TiO_2 was composed of Ti, O and N. Further, N was doped into the TiO_2 lattice by substituting for O, forming the oxidized nitrogen in the form of Ti–N–O or Ti–O–N bond, and Ti was present in the form of Ti^{4+} in TiO_2. Finally, the absorbance of N−doped TiO_2 was obviously improved in both UV and visible light region. Optical absorption edges of N−doped TiO_2 samples showed obvious red shift, which expanded spectral absorption range of TiO_2 and improved the utilization efficiency of visible light. It is concluded that N element was successfully doped into TiO_2 crystal lattice, and the N dopant concentration of 3.0% was designed to modify TiO_2.

Key words: titanium dioxide; nitrogen doping; microstructures; optical properties; photocatalytic activity

1 Introduction

Titanium dioxide (TiO_2), as a photocatalyst, was widely concerned because of its excellent photochemical properties, high photostability, low cost and nontoxicity[1]. TiO_2 has been used in water treatment, air purification, solar energy harvesting and so on[2,3]. However, TiO_2 can only absorb the ultraviolet (UV) light due to its wide band gap[4]. Consequently, the photocatalytic activity of TiO_2 is only activated by the UV fraction which represents about 4% of the total sun irradiance. This limits the photocatalytic efficiency of TiO_2 and the full utilization of solar energy[5]. Another drawback of conventional pure TiO_2 is that the photo-generated carriers may recombine due to illumination on the surface and inside of TiO_2 particles which also reduces the photocatalytic activity of TiO_2[6]. So how to improve the photocatalytic efficiency under visible light irradiation and quantum efficiency of TiO_2 has become one of important aspects for this photocatalyst[7,8].

Recently, it is necessary to modify the TiO_2 to facilitate visible light absorption to make full use of sunlight. Many approaches, such as ion doping, surface precious metal deposition, composite semiconductor, *etc*, were used to shift the optical absorption edges of TiO_2 to the visible light region[9] for improving the photocatalytic activity of TiO_2 and the utilization efficiency of visible light[10]. Among these opproaches, the ion doping also included metal and nonmetal ion doping[11]. The metal doping was utilized to dope the ions into the TiO_2 lattice for substituting Ti^{4+}, and the doping energy level was introduced to the band gap of TiO_2, which could extend the absorption edges to visible light region[12]. Similarly, the doping can enable nonmetal ions to enter into the TiO_2 lattice for substituting O^{2-}, which generated a new impurity level to narrow the band gap in TiO_2, and improve the absorption efficiency of visible light[13].

However, the metal doping has its own disadvantages[14]. For example, the metal doping affects the thermal stability of TiO_2, and provides recombination points for photo-generated carriers. In addition, the

(Received: Nov. 14, 2017; Accepted: Oct. 25, 2018)

XU Tao (许涛): Prof.; Ph D; E-mail: seuxt@163.com

Funded by National Natural Science Foundation of China (No. 51378264), Open Research Fund of National Engineering Laboratory for Advanced Road Materials (No. NLARM-ORF-2018-02) and Provincial Six Talent Peaks Project in Jiangsu, China (No. JNHB-050)

metal doping requires expensive ion implantation equipments, and the metal ions may affect the photocatalytic activity of TiO_2 in the UV light region[14]. Also, the metal oxide generated during the preparation of TiO_2 nanoparticles reduces their effective specific surface areas[15]. Therefore, it is important to develop a more effective method to enhance the photocatalytic activity of TiO_2.

It was noted that the impurity level of nonmetal ion doping was close to the conduction band of TiO_2, and the nonmetal doping could narrow the band gap of TiO_2[16]. This not only contributed to improve the photocatalytic activity of TiO_2 in visible light region, but also affected its photocatalytic activity in the UV region. So many attentions were paid to the nonmetal doping of TiO_2[17]. The nonmetal doping of TiO_2 has shown great promise in achieving photocatalysis, and the N has becomes one of the most promising dopants[18]. Compared with other nonmetal doping, N-doped TiO_2 showed a significant photocatalytic activity and strong absorption under visible light irradiation[19].

So far, many efforts have been focused on the research of N-doped TiO_2 because of its high photocatalytic activity, low fabrication cost and controllable synthesis[20]. Further, the decrease in band gap through the N doping also has been studied extensively with different approaches. Some nitriding techniques have been developed to synthesize N-doped TiO_2, such as sol-gel, ammonolysis, hydrothermal and solvothermal combined with post-nitriding[21,22]. As a conventional method, the sol-gel method is facile and inexpensive to synthesize N-doped TiO_2.

Jiang *et al*[23] found that the N doping could efficiently narrow the band gap of TiO_2 and created the oxygen vacancy. Behnajady *et al*[24] prepared TiO_2 nanoparticles, and discussed their crystalline phase, particle size and photocatalytic activity. Lee *et al*[25] reported the synthesis of nanoporous N-TiO_2 with an anatase crystalline structure by modifying sol-gel method and ultrasound irradiation. Todorova *et al*[26] prepared the N-doped TiO_2 nanopowders, and discussed beneficial effects of N-doping on the photocatalytic activity of TiO_2. Powell *et al*[27] described a reliable and effective method for incorporating N via a bidentate chelating ligand. Ramchiary *et al*[28] studied the photocatalytic performance of hydrogenated N doped mixed phase titania under visible light irradiation.

It was found that how N doping enhances the photocatalytic activity of TiO_2 under visible light irradiation has not been observed although the general agreement was obtained regarding the improvement in photocatalytic activity of TiO_2[29]. Therefore, there was an on-going discussion on how the N doping enhances the photocatalytic activity of TiO_2 under visible light irradiation[30]. Additionally, the effects of N doping on electronic structures and optical properties of TiO_2 nanomaterials were still in discussion[30]. The objective of this study was to modify the TiO_2 using nonmetal N as dopant, and confirm the N ions were doped into TiO_2 lattice structures through different characterization methods, improving the photocatalytic activity of TiO_2 under visible light irradiation. The photocatalytic mechanism of N-doped TiO_2 under visible light irradiation was also discussed.

In this study, the N-doped TiO_2 nanopowders containing different N dopant concentrations were synthesized by sol-gel method. The phase structure and components of the synthesized TiO_2 samples were characterized by XRD, and the effects of N doping on the microcosmic lattice structure and morphology of TiO_2 were discussed based on TEM and HRTEM tests. Additionally, the electronic structure, chemical composition and optical properties of the TiO_2 samples were investigated by XPS and UV-Vis DRS to discuss the reasons for the improvement in photocatalytic activity of N-doped TiO_2 under that visible light irradiation. The test results from the above characterization methods were used to confirm that N element was successfully doped into the TiO_2 crystal lattices.

2 Experimental

2.1 Synthesis of TiO_2 samples

The sol-gel method was utilized to synthesize N-doped TiO_2 nanoparticles using tetra-n-butyl titanate and carbamide as titanium and N precursor, respectively. Firstly, 30 mL anhydrous alcohol was blended with 17 mL tetra-n-butyl titanate in a glass beaker at room temperature, and the constant stirring was kept for 30 min to form a homogeneous and yellowish solution, which was named solution A. Secondly, 28 mL anhydrous alcohol, 20 mL acetic acid and 8 mL deionized water were blended in another glass beaker at room temperature, and then a certain quantity of carbamide (the mole ratio of N/Ti was 1.0%, 2.0%, 3.0% and 4.0%, respectively) were added into the mixed liquor. After fully mixing, the resultant mixed liquor was named solution B.

Thirdly, solution B was added into solution A at the speed of one or two drops per second with magnetic stirring at 30℃ to obtain the uniform and transparent sol, and then the sol was matured for 7 days at room temperature to form gel. Finally, the gel was dried for 24 h at 80 ℃, and then was grinded into powders and calcined for 2.5 h at 400 ℃ to obtain N-doped TiO_2 nanoparticles which was expressed as TiO_2+NX (the X represented the N dopant concentration in N−doped TiO_2). According to the above discribed method, the N−doped TiO_2 with different N dopant concentrations were synthesized, and the carbamide was not added into the mixed liquor in the second step to prepare pure TiO_2 nanopowders.

2.2 Characterization methods

An X-ray diffractometer (Ultima IV type, Rigaku, Japan) was used to characterize the phase microstructures and composition of synthesized TiO_2 samples. The XRD analyzer was with Cu-$K\alpha$ radiation (λ=0.154 18 nm). The accelerating voltage and applied current were 40 kV and 30 mA, respectively. The XRD patterns were recorded in the 2θ range from 10° to 80° in the step scan mode at a rate of 2 °/min.

The morphology and microstructure of the prepared TiO_2 samples were observed by field emission TEM (JEM-2100 (HR) type, JEOL, Japan). Its point resolution was 0.23 nm, and the lattice resolution is 0.14 nm, and the amplification times was 50-1 500 000.

The electronic structure and chemical composition of TiO_2 samples were analyzed by XPS (AXIS Ultra DLD type, Shimadzu, Japan) with the monochromatized Al-$K\alpha$ (hv=1 486.6 eV) radiation as an excitation source. The accelerating voltage and applied current were 15 kV and 20 mA, respectively, and the vacuum degree was 10^{-8} Torr. The adventitious carbon (C1*s* peak at 284.8 eV) was used to calibrate the binding energy.

A UV-vis spectrophotometer (Lambda 950 type, PE, USA) equipped with an integrating sphere was utilized to record the diffuse reflectance spectra of TiO_2 samples. A $BaSO_4$ standard was used as a reference sample for baseline correction. The scan range was 200-800 nm at a data interval of 1 nm.

3 Results and discussion

3.1 Phase structure and component analysis

XRD was used to investigate the crystal phase structures of TiO_2 samples and the structural effects of N−doping. The XRD patterns of synthesized TiO_2 samples with different N dopant concentrations are illustrated in Fig.1.

From Fig.1, the XRD patterns show similar phases between the pure and N−doped TiO_2 because of a small amount of N dopant concentration. It is observed that six different typical diffraction peaks at 25.3°, 37.8°, 48.0°, 53.9°, 55.0° and 62.7° correspond to the crystal planes of (101), (004), (200), (105), (211) and (204), respectively. Compared with the TiO_2 standard card (JCPDS NO: 21-1272), all N-doped TiO_2 samples are anatase phase, and the characteristic peaks associated with the rutile phase are not observed. This confirms the high purity and crystallinity of synthesized TiO_2. Additionally, compared with the pure TiO_2, the phase composition of N-doped TiO_2 samples are almost unchanged. It is also seen that the peak positions of major diffraction patterns of the N doped TiO_2 had similar values as that of pure TiO_2, except the changes in intensities of the above peaks.

Furthermore, the diffraction peaks of impurities related to N in the XRD patterns are not observed, which indicates that N element does not agglomerate to reach the macro level. Also, the doped N ions are uniformly dispersed in the lattice structures of TiO_2, and its influence on the microstructures of TiO_2 is negligible. It is concluded that the N doping does not affect the crystal phase structures of TiO_2 samples. Phase structure parameters of pure and N-doped TiO_2 are summarized in Table 1. The average crystallite sizes of TiO_2 samples are calculated according to the Debye-

Table 1 Phase structure parameters of pure and N-doped TiO_2 samples

Samples	Crystallite size/nm	FWHM	Micro strain	Lattice parameters/Å	
				a=*b*	*c*
Pure−TiO_2	16.0	0.544	0.362 3	3.788	9.514
TiO_2+N1.0%	14.5	0.549	0.378 1	3.788	9.514
TiO_2+N2.0%	14.4	0.556	0.408 9	3.786	9.512
TiO_2+N3.0%	13.5	0.569	0.409 0	3.784	9.511
TiO_2+N4.0%	14.3	0.560	0.430 1	3.781	9.514

Scherrer equation based on the main (101) diffraction peak[31].

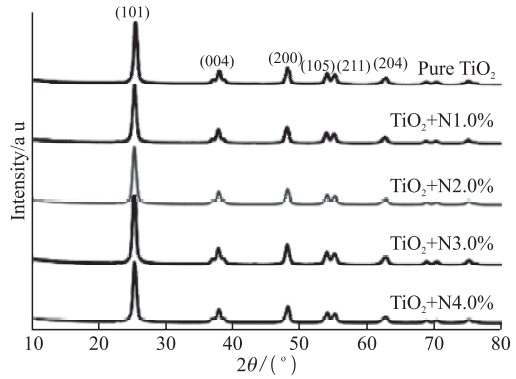

Fig.1 XRD patterns of synthesized TiO_2 samples with different N dopant concentrations

As shown in Table 1, the crystallites sizes of synthesized TiO_2 nanoparticles are in the range of 13-16 nm. The crystallite sizes of N-doped TiO_2 samples are less than that of the pure TiO_2, which is due to the fact that the N dopant penetrates into the crystal lattice of TiO_2 and reduces the crystallite size. However, the crystallite sizes of N-doped TiO_2 samples first show a decreasing and then increasing trend with the increase in N dopant concentrations from 1.0% to 4.0%. The crystallite size of N-doped TiO_2 sample is the smallest at the N dopant concentration of 3.0%. On the contrary, the full width at half maximum (FWHM) in XRD patterns of N-doped TiO_2 samples first shows an increasing and then decreasing trend with the increase in N dopant concentration from 1.0% to 4.0%. This indicates that the N doping inhibits the crystallite growth of TiO_2, and the inhibiting effect at the N dopant concentration of 3.0% is more obvious.

Additionally, it is found from Table 1 that the lattice structure parameters of TiO_2, such as *a*, *b* and *c*, show somewhat changes. The lattice parameters, *a* and *b*, always show a decreasing trend, and *c* first presents a decreasing and then increasing trend with the increase in N dopant concentration. This implies that the internal crystal structures of TiO_2 are affected by the N doping, and the higher N dopant concentration, the greater TiO_2 lattice changes. This also results in the lattice distortion in TiO_2. It is seen that the micro strain of lattice gradually increases with the increase in N dopant concentration, which suggests that the N elements are doped into the crystal lattices of TiO_2, leading to the increase in micro strain of TiO_2.

This is because the anatase crystal lattice contains more defects and dislocations, which generate more oxygen vacancies to capture the electrons, and thus it is difficult to recombine for photo-generated electrons and holes[32]. All these factors improve the photocatalytic activity of anatase phase. These findings are consistent with the previous research results[32]. In addition, the ionic radius of N^{3-} (0.013 nm) is similar to that of O^{2-} (0.014 nm), so it is easy for N to substitute O from the crystal lattice and form N–O, Ti–N and impurity levels[32]. XRD results reveal that N species have been incorporated into the TiO_2 lattice to substitute the O^{2-}. All these are conducive to improve the photocatalytic activity of N–doped TiO_2.

3.2 Morphology and microstructure analysis

TEM and HRTEM were used to analyze the effects of N doping on the dispersity, morphology and microcosmic lattice structure of TiO_2. TEM images of N–doped TiO_2 samples are shown in Fig.2.

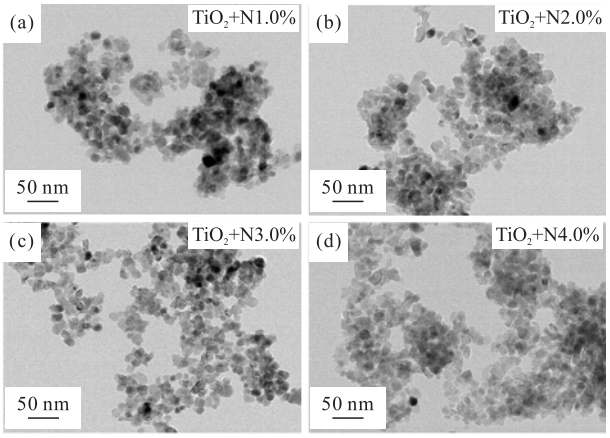

Fig.2 TEM images of N–doped TiO_2 samples with different N dopant concentrations

As shown in Fig.2, the morphologies of N–doped TiO_2 samples present the spherical nanoparticles. The crystallite size range of TiO_2 is in the range of 13-16 nm, which is in accord with the results from XRD. Also, it is intuitively observed that the dispersity of TiO_2 nanoparticles is improved with the increase in N dopant concentration from 1.0% to 4.0%. The reason is that the N-doping reduces the agglomeration of TiO_2 nanoparticles during heat treatment to improve the dispersibility. This also increases the specific surface area of TiO_2 nanoparticles, which is helpful to improve the photocatalytic activity of TiO_2.

To further investigate the microcosmic lattice structure of N-doped TiO_2, the N-doped TiO_2 sample with the N concentration of 3.0% (namely TiO_2+N3.0% sample) are taken as an example to discuss its HRTEM images, FFT diagram and SAED pattern as shown in Fig.3.

Fig.3 (a) shows the HRTEM image of TiO_2+N3.0% sample. The crystallites have clearly highly

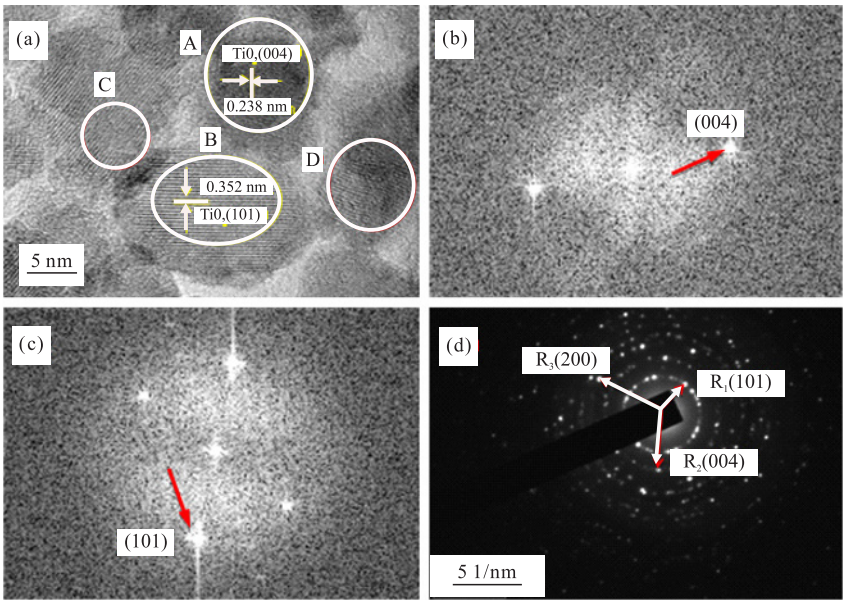

Fig.3 HRTEM image, FFT diagram and SAED pattern of TiO_2+N3.0% sample: (a) HRTEM image, (b) FFT diagram of region A, (c) FFT diagram of region B and (d) SEAD pattern

ordered lattice fringes spaced at 0.352 and 0.238 nm, corresponding to the crystal planes of (101) and (004) in the anatase, respectively. This proves the high crystallinity of the N-doped TiO_2 sample. Also, the obvious distorted lattice fringes are observed at region C and D in Fig.3 (a). This suggests that the N ions are doped in TiO_2 lattice structure and leads to the TiO_2 lattice distortion which forms lattice defects, which is consistent with the XRD results. Region A and B are corresponding to the lattice plane (101) and (004) in the anatase, and whose interplanar spacings are 0.352 and 0.238 nm, respectively[33]. Fig.3 (b) and (c) are the fast Fourier transform (FFT) diagram of region A and B in Fig.3 (a), respectively. The existence of lattice plane (101) and (004) in the N-doped TiO_2 sample are further verified through the calibration of FFT diagrams of region A and B as shown in Fig.3 (b) and (c), respectively.

From Fig.3 (d), the high crystallization degree of TiO_2+N3.0% sample is shown by the bright spots, forming well-defined diffraction rings in the selected areas of electron diffraction (SAED) patterns. The electron diffraction patterns of N-doped TiO_2 samples are observed which are the (101), (004), and (200) diffractions of the polycrystals with the anatase phase. The concentric rings were encircled with dotted circular outlines to identify the crystalline planes. The radiuses (R) of different electron diffraction rings are measured to obtain the interplanar spacings (d) through the reciprocal of R, respectively. According to the d values and the TiO_2 standard card, it is found that such characteristic rings as R_1, R_2 and R_3 in the SAED pattern were assigned to the diffractions from the lattice plane (101), (004) and (200), respectively. The above lattice planes correspond to the interplanar spacings of 0.352, 0.238 and 0.189 nm, respectively. This also further validates the crystal structure of synthesized N–doped TiO_2 is anatase phase.

3.3 Electronic structure and chemical composition analysis

XPS was used to discuss the electronic structure, chemical compositions and element valence state of TiO_2+N3.0% sample. The XPS survey spectrum and high resolution XPS (HRXPS) spectra of the characteristic elements in N–doped TiO_2 sample are shown in Fig.4.

From Fig.4 (a), the XPS survey spectrum of TiO_2+N3.0% sample shows the existence of different elements, including Ti, O, N and C. Among these, the C1s peak at 284.8 eV is possibly ascribed to the remaining precursor not yet completely removed at 400 ℃ due to the introduced impurities or the absorption of CO_2 during the sample preparation. Fig.4 (b) shows the HRXPS spectra of Ti2*p* state in N–doped and pure TiO_2 samples, and which both consist of double peaks. The observed broad peak at around 464.1 eV and the sharp narrow peak at around 458.4 eV for both N-doped and pure TiO_2 sample suggest the presence of Ti and Ti^{4+} species[34]. These peaks are attributed to an active site which improves the photocatalytic activity, especially under visible light irradiation[35].

The XPS peaks at the binding energy of 464.1

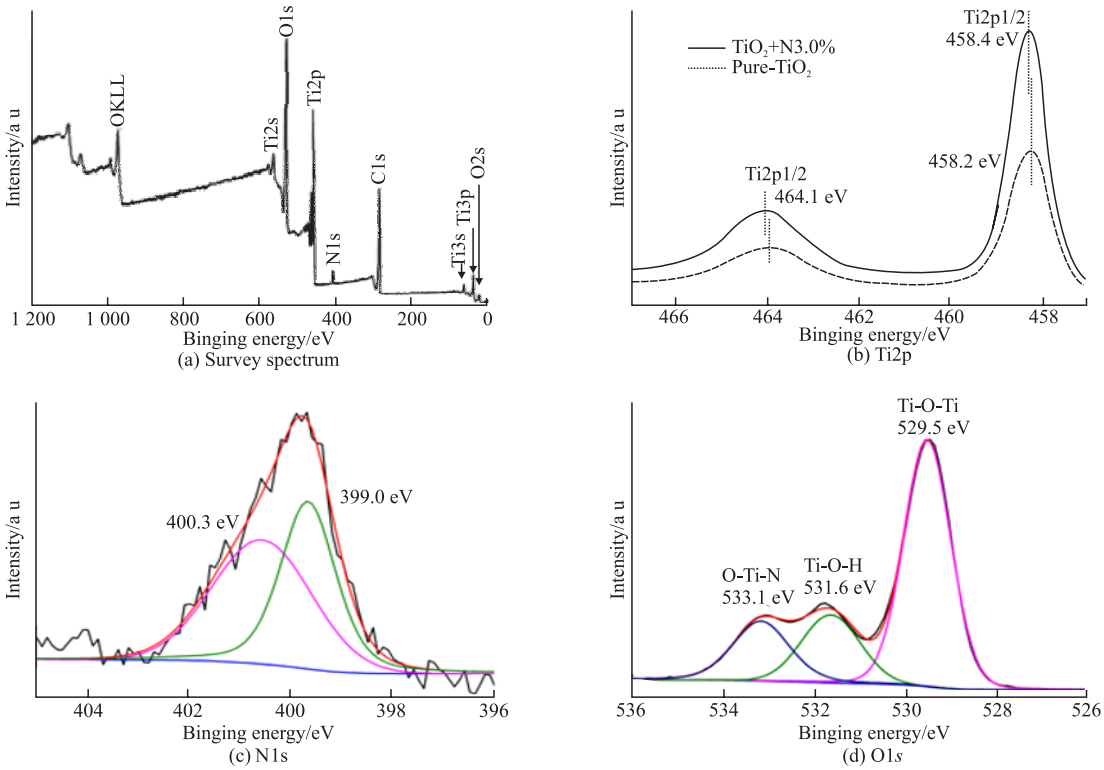

Fig.4 XPS survey spectrum and HRXPS spectra of characteristic elements in N–doped TiO_2

and 458.4 eV are assigned to $Ti2p_{1/2}$ and $Ti2p_{3/2}$ states of N-doped TiO_2 with a chemical shift of 5.7 eV, respectively. This indicates that Ti is present in the form of Ti^{4+}[36]. Also, it is noted that the binding energy values at the two peaks of Ti2*p*1/2 and Ti2*p*3/2 in the pure TiO_2 sample are 463.9 and 458.2 eV, respectively, which are both somewhat less than that in the N-doped TiO_2. This is because that the N doping causes the Ti atoms to lose some outer layer electrons, leading to a change in the lattice structure of TiO_2[36], which is consistent with the results of XRD characterization.

Fig.4 (c) presents the HRXPS spectra of N1s state in N-doped TiO_2 sample. Two XPS spectra peaks at the binding energy of 399.0 and 400.3 eV are obtained through the peak–fit processing. The binding energy range of N1s peaks is 396–404 eV, which is considered as the typical characteristic of N-doped TiO_2[37]. The binding energy peaks at 399.0 and 400.3 eV can be attributed to the oxidized nitrogen in the form of Ti–N–O and/or Ti–O–N bonds[38,39]. The reason is that O is substituted by N in the crystal lattice of N–doped TiO_2 and the electronegativity of O is greater than that of N[38]. Consequently, O in Ti–N–O and/or Ti–O–N lowers the electron cloud density of the valence orbit in N atoms so as to weaken the shielding effect to inner orbit[38]. The interaction between the inner orbit electrons and the nucleus is enhanced, resulting in the increase in orbit binding energy on XPS spectra. This further indicates that the N species have been incorporated into the TiO_2 lattice[39].

Fig.4 (d) shows the HRXPS spectra of O1s state in N–doped TiO_2 sample. The binding energy range of N1s peaks is 528-535 eV, including three peaks at the binding energy of 529.5, 531.6 and 533.1 eV, respectively. The first peak at the binding energy of 529.5 eV is corresponding to the combined oxygen in TiO_2 lattice which occurs in the form of Ti–O–Ti[40]. The second peak at the binding energy of 531.6 eV belongs to the surface adsorbed oxygen which exits in the form of Ti–O–H. The last peak at the binding energy of 533.1eV is attributed to the O1s presence in O–Ti–N bond[41]. The HRXPS spectra of N1s and O1s state show that the O is substituted by N in the TiO_2 lattice, and the N is doped into the TiO_2 lattice.

3.4 Optical property analysis

In order to study the influence of N doping on the optical properties of TiO_2, the UV-vis DRS test results were recorded on different synthesized TiO_2 samples. The test results are illustrated in Fig.5.

As shown in Fig.5, the absorbance of N-doped TiO_2 is obviously improved in both UV and visible light region when compared with the pure TiO_2. Further, the optical absorption edges of N-doped TiO_2 samples show red shift, and the TiO_2+N3.0% sample presents

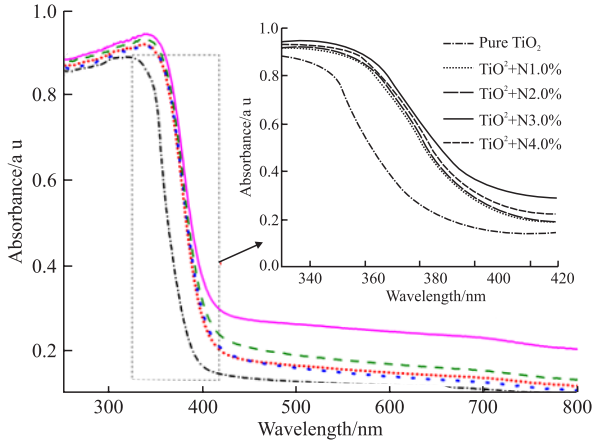

Fig.5 UV-Vis DRS of pure and N–doped TiO_2 samples with different N dopant concentration

Table 2 Maximum absorption wavelength edge and E_g of N-doped TiO_2 samples

Samples	Pure-TiO_2	TiO_2+N1.0%	TiO_2+N2.0%	TiO_2+N3.0%	TiO_2+N4.0%
λ/nm	390	407	409	416	412
E_g/eV	3.18	3.04	3.03	2.98	3.01

the most obvious red shift (Fig.5). This indicates that the N-doping extends the optical absorption range of TiO_2 from UV to visible light region, which increases the photocatalytic degradation efficiency and expands the application range of TiO_2. The reason is that the N introduction forms the local intermediate band gap (N2p) energy level on the top of O2p valence band in TiO_2[43]. Electrons of the doping energy level can be motivated to the conduction band of TiO_2, causing the long wave photons to be absorbed[21]. Thus the absorption spectrum range of TiO_2 is extended to the visible light region and the absorption properties in the visible light region are improved.

To further study the change in band gap of TiO_2 samples, the intercept of the tangents to the plots of $(\alpha hv)^2$ *vs* photon energy (hv) is shown in Fig.6 when TiO_2 is considered as an indirect semiconductor[42]. According to semiconductor optical absorption theory, the optical band gap values of TiO_2 samples can be calculated based on Eq. (1).

$$(\alpha hv)^2 = B(hv - E_g) \tag{1}$$

where α is the absorption coefficient, h is the Planck's constant, v is the light frequency, and B is a constant.

The $(ahv)^2$ is used as a function of photon energy, and the linear part of the curve is extended to the horizontal axis[43]. The intersection points on horizontal axis are the band gap of TiO_2 samples as shown in Fig.6.

Then according to Eq.(2), the relationship between the maximum absorption wavelength edge (λ) and E_g is determined as given in Table 2 [43].

$$E_g = 1\,240/\lambda \tag{2}$$

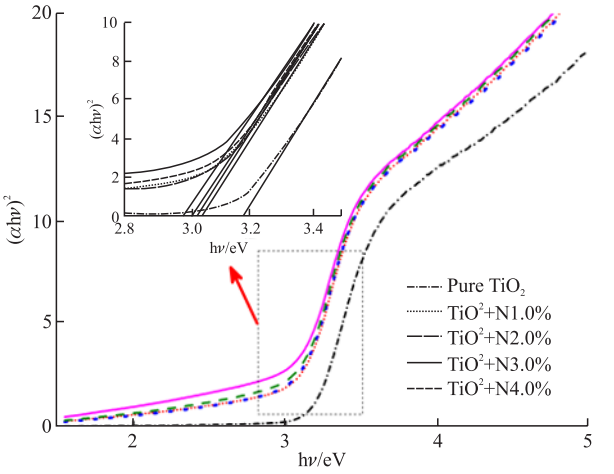

Fig.6 Optical absorption edges of pure and N–doped TiO_2 samples with different N dopant concentrations

From Table 2, when the N dopant concentration is less than 3.0%, the E_g values of TiO_2 samples decrease with the increase in N dopant concentration, indicating a red shift to the visible light region. However, when the N dopant concentration is more than 3%, the E_g values of TiO_2 samples increase with the increase in N dopant concentration. It is concluded that the TiO_2 sample with the N dopant concentration of 3% shows a better absorption property of visible light.

The decrease in band gap of N–TiO_2 is attributed to the presence of interstitial N in the TiO_2 matrix [44]. The N doping creates N2p energy states in the maximum valance band and the electronic transitions

occur from the N2p level to the conduction band of TiO_2 [45]. Additionally, it is believed that the changes in optical absorption edge and E_g of TiO_2 samples are related to the doped N, and the N dopant concentration affects the visible light absorption of TiO_2. This also implies that N element is successfully doped into TiO_2 crystal lattice and the optical absorption of TiO_2 in the visible light region can be enhanced by N−doping.

4 Conclusions

a) Pure and N-doped TiO_2 samples were synthesized by sol-gel method, and their crystals only contain anatase phase with a slight distortion. The N dopant is uniformly dispersed in the lattice structure of TiO_2, not affecting the crystal phase structures of TiO_2. The crystallite sizes of TiO_2 nanoparticles increase first and then decrease in the range of 13-16 nm with the increase in N dopant concentration.

b) Morphology and microstructures studies show that the dispersity of prepared TiO_2 nanoparticles is improved with the increase in N dopant concentration. HRTEM images confirm that the N ions are doped in TiO_2 lattice structure and leads to the TiO_2 lattice distortion. The N doping brings more defects in TiO_2, which can capture charge carriers and inhibit obviously the combination of electrons and holes.

c) The XPS spectra suggest that the prepared TiO_2 sample contains three elements, including Ti, O and N. And N elements are doped into the TiO_2 lattice, forming the oxidized nitrogen in the form of Ti–N–O or Ti–O–N bond. HRXPS spectra suggest that Ti is present in the form of Ti^{4+} in TiO_2, and N is doped into the TiO_2 lattice by substituting O in the TiO_2 lattice.

d) The absorbance of N-doped TiO_2 is improved in both UV and visible light region. The optical absorption edges of N-doped TiO_2 samples show obvious red shift, and the most obvious red shift is observed corresponding to a higher band gap value when N dopant concentration is 3.0%. The absorption of TiO_2 in visible light region is enhanced by N-doping, expanding the absorption spectral range of TiO_2 and improving the utilization efficiency of visible light.

e) It is believed that N element is successfully doped into TiO_2 crystal lattice confirmed by XRD, TEM, HRTEM, XPS and UV-vis DRS. The N dopant concentration of 3.0% was designed to modify TiO_2. The synthesized N-doped TiO_2 has higher photocatalytic activity and degradation efficiency in visible light region, which extends the potential applications of N−doped TiO_2 in water treatment, air purification, *etc*.

Acknowledgements

Authors would like to thank Advanced Analysis & Testing Center of Nanjing Forestry University for the assistance in experiments.

References

[1] Li H, Hao YB, Lu HQ. A Systematic Study on Visible-Light N-Doped TiO_2 Photocatalyst Obtained from Ethylenediamine by Sol-Gel Method[J]. *Appl. Surf. Sci.*, 2015, 344: 112-118

[2] Chen ML, Oh WC. The Improved Photocatalytic Properties of Methylene Blue for V_2O_3/CNT/TiO_2 Composite under Visible Light[J]. *Int. J. Photoenergy*, 2010, 4: 424-448

[3] Lv K, Xiang Q, Yu J. Effect of Calcination Temperature on Morphology and Photocatalytic Activity of Anatase TiO_2 Nanosheets with Exposed (001) Facets[J]. *Appl. Cataly. B*, 2011, 104 (3): 275-281

[4] Lu HQ, Yao JF. Recent Advances in Liquid-Phase Heterogeneous Photocatalysis for Organic Synthesis by Selective Oxidation[J]. *Curr. Org. Chem.*, 2014, 18 (10): 1 365-1 372

[5] Veluru JB, Appukuttan SN, Zhu PN. Synthesis and Characterization of Rice Grains Like Nitrogen-Doped TiO_2 Nanostructures by Electrospinning-Photocatalysis[J]. *Mater. Lett.*, 2011, 65 (19-20): 3 064-3 068

[6] Daghrir R, Drogui P, Robert D. Modified TiO_2 for Environmental Photocatalytic Applications: a Review[J]. *Ind. Eng. Chem. Res.*, 2013, 52 (10): 3 581-3 590

[7] Macwan DP, Dave PN, Chaturvedi S. A Review on Nano-TiO_2 Sol-Gel Type Syntheses and Its Applications[J]. *J. Mater. Sci.*, 2011, 46 (1): 3 669-3 686

[8] Cui XL, Li YG, Zhang QH. Silver Orthophosphate Immobilized on Flaky Layered Double Hydroxides As the Visible-Light-Driven Photocatalysts[J]. *Int. J. Photoenergy*, 2012, 1110-662X: 1 302-1 312

[9] Wang Y, He Y, Lai Q. Review of the Progress in Preparing Nano TiO_2: An Important Environmental Engineering Material[J]. *J. Envir. Sci.*, 2014, 26 (11): 2 139-2 177

[10] Pang YL, Lim S, Ong HC. A Critical Review on the Recent Progress of Synthesizing Techniques and Fabrication of TiO_2-Based Nanotubes Photocatalysts[J]. *Appl. Catal. A-Gen.*, 2014, 481(25): 127-142

[11] Gu D, Zhu Y, Xu Z. Effects of Ion Doping on the Optical Properties of Dye-Sensitized Solar Cells[J]. *Adv. Mater. Phys. Chem.*, 2014, 4 (10): 187-193

[12] Banerjee AN. The Design, Fabrication, and Photocatalytic Utility of Nanostructured Semi- Conductors: Focus on TiO_2-Based Nanostructures[J]. *Nanotech. Sci. Appl.*, 2011, 4: 35-65

[13] Silija P, Yaakob Z, Suraja V. An Enthusiastic Glance in to the Visible Responsive Photocatalysts for Energy Production and Pollutant Removal, with Special Emphasis on Titania[J]. *Int. J. Photoenergy*, 2012, 44 (1): 90-99

[14] Mallakpour S, Nikkhoo E. Surface Modification of Nano-TiO_2 with

Trimellitylimido-Amino Acid-Based Diacids for Preventing Aggregation of Nanoparticles[J]. *Adv. Powder Technol.*, 2014, 25 (1): 348-353

[15] Dong H, Zeng G, Tang L. An Overview on Limitations of TiO_2-Based Particles for Photocatalytic Degradation of Organic Pollutants and the Corresponding Countermeasures[J]. *Water Res.*, 2015, 79: 128-146

[16] Ohno T, Murakami N. Develpoment of Metal Cation Compound-Doped TiO_2 Photocatalysts Having a Rutile Phase under Visible Light[J]. *Appl. Catal. A-Gen.*, 2008, 349 (1): 70-75

[17] Li FF, Jing YS, Xia MS. Effect of the P/Ti Ratio the Visible-Light Photocatalytic Activity of P-Doped TiO_2[J]. *J. Phys. Chem. C*, 2009, 113 (42):18 134-18 141

[18] Fujishima A, Zhang X, Tryk DA. TiO_2 Photocatalysis and Related Surface Phenomena[J]. *Surf. Sci. Rep.*, 2009, 63 (12): 515-582

[19] Gomathi Devi L, Kavitha R. A Review on Nonmetal Ion Doped Titania for the Photocatalytic Degradation of Organic Pollutants under UV/Solar Light: Role of Photogenerated Charge Carrier Dynamics in Enhancing the Activity[J]. *Appl. Catal. B-Environ.*, 2013, s140-141(8): 559-587

[20] Mamane H, Horovitz I, Lozzi L. The Role of Physical and Operational Parameters in Photocatalysis by N-Doped TiO_2 Sol-Gel Thin Films[J]. *Chem. Eng. J.*, 2014, 257 (6): 159-169

[21] Yang G, Jiang Z, Shi H. Preparation of Highly Visible-Light Active N-Doped TiO_2 Photocatalyst[J]. *J. Mater. Chem.*, 2010, 20 (25): 5 301-5 309

[22] Chen X, Mao SS. Titanium Dioxide Nanomaterials: Synthesis, Properties, Modifications, and Applications[J]. *Chem. Rev.*, 2007, 38 (41): 2 891-2 959

[23] Jiang Z, Kong L, Alenazey FS. Enhanced Visible-Light-Driven Photocatalytic Activity of Mesoporous TiO_2-*x*N*x* Derived from the Ethylenediamine-Based Complex[J]. *Nanoscale*, 2013, 5 (12): 5 396-5 402

[24] Behnajady MA, Eskandarloo H, Modirshahla N. Investigation of the Effect of Sol-Gel Synthesis Variables on Structural and Photocatalytic Properties of TiO_2 Nanoparticles[J]. *Desalination*, 2011, 278 (1-3): 10-17

[25] Lee HU, Lee SC, Choi S. Efficient Visible-Light Induced Photocatalysis on Nanoporous Nitrogen-Doped Titanium Dioxide Catalysts[J]. *Chem. Eng. J.*, 2013, 228 (14): 756-764

[26] Todorova N, Vaimakis T, Petrakis D. N and N, S-Doped TiO_2 Photocatalysts and Their Activity in NO_x Oxidation[J]. *Catal. Today*, 2013, 209 (12): 41-46

[27] Powell MJ, Dunnill CW, Parkin IP. N-Doped TiO_2 Visible Light Photocatalyst Films via a Sol-Gel Route Using TMEDA As the Nitrogen Source[J]. *J. Photochem. Photob. A: Chem.*, 2014, 281 (5): 27-34

[28] Ramchiary A, Samdarshi SK. Hydrogenation Based Disorder-Engineered Visible Active N-Doped Mixed Phase Titania[J]. *Solar Ener. Mater. Solar Cell*, 2015, 134: 381-388

[29] Monteiro RAR, Miranda SM, Vilar VJP. N-Modified TiO_2 Photocatalytic Activity Towards Diphenhydraminedegradation and Escherichia Coli Inactivation in Aqueous Solutions[J]. *Appl. Catal. B- Envir.*, 2015, 162 (6): 66-74

[30] Emeline AV, Sheremetyeva NV, Khomchenko NV. Photoinduced Formation of Defects and Nitrogen Stabilization of Color Centers in N-Doped Titanium Dioxide[J]. *J. Phys. Chem. C*, 2007, 111 (30): 11 456-11 462

[31] Lee K, Kim D, Roy P. Anodic Formation of Thick Anatase TiO_2 Mesosponge Layers for High-Efficiency Photocatalysis[J]. *J. Am. Chem. Soc.*, 2010, 132 (5): 1 478-1 489

[32] Pelaez M, Nolan NT, Pillai SC. A Review on the Visible Light Active Titanium Dioxide Photocatalysts for Environmental Applications[J]. *Appl. Catal. B- Envir.*, 2012, 125 (33): 331-349

[33] Dong F, Guo S, Wang H. Enhancement of the Visible Light Photocatalytic Activity of C-Doped TiO_2 Nanomaterials Prepared by a Green Synthetic Approach[J]. *J. Phys. Chem. C*, 2014, 115 (27): 13 285-13 292

[34] Leong KH, Monash P, Ibrahim S. Solar Photocatalytic Activity of Anatase TiO_2 Nanocrystals Synthesized by Non-Hydrolitic Sol-Gel Method[J]. *Solar Energy*, 2014, 101(1): 321-332

[35] Aziz AA, Puma GL, Ibrahim S. Preparation, Characterisation and Solar Photoactivity of Titania Supported Strontium Ferrite Nanocomposite Photocatalyst[J]. *J. Exp. Nanosci.*, 2013, 8 (3): 295-310

[36] Ma W, Wang Q, Qin Z. Green Synthesis of Silver-Modified TiO_2 Hollow Spheres and Their Visible Photocatalytic Performance[J]. *J. Chen, J. Univer. Jinan*, 2016, 30: 167-176

[37] Ou HH, Luo SL, Liao CH. N-Doped TiO_2 Prepared from Microwave-Assisted Titanate Nanotubes ($Na_xH_{2-x}Ti_3O_7$): the Effect of Microwave Irradiation during TNT Synthesis on the Visible Light Photoactivity of N-Doped TiO_2[J]. *J. Phys. Chem. C*, 2011, 115 (10): 4 000-4 007

[38] Li H, Li J, Huo Y. Highly Active TiO_2 N Photocatalysts Prepared by Treating TiO_2 Precursors in NH_3/Ethanol Fluid under Supercritical Conditions[J]. *J. Phys. Chem. B*, 2006,110(4): 1 559-1 565

[39] Yang X, Cao C, Erickson L. Photo-Catalytic Degradation of Rhodamine B on C-, S-, N-, and Fe-Doped TiO_2 under Visible Light Irradiation[J]. *Appl. Catal. B-Envir.*, 2009, 91(3-4): 657-662

[40] Emeline AV, Kuznetsov VN, Rybchuk VK. Visible-Light-Active Titania Photocatalysts: the Case of N-Doped TiO_2-Properties and Some Fundamental Issues[J]. *Int. J. Photoenergy*, 2008, 4: 1-19

[41] Chen XB, Burda C. Photoelectron Spectroscopic Investigation of Nitrogen-Doped Titania Nanoparticles[J]. *J. Phys. Chem. B*, 2004, 108 (40): 15 446-15 449

[42] Zhang J, Fu WJ, Xi J. N-doped Rutile TiO_2 Nano-Rods Show Tunable Photocatalytic Selectivity[J]. *J. Alloy. Compd.*, 2013, 575 (20): 40-47

[43] Kuo C, Wu C, Wu J, *et al*. Synthesis and Characterization of a Phosphorus-Doped TiO_2 Immobilized Bed for the Photodegradation of Bisphenol A under UV and Sunlight Irradiation[J]. *Reac. Kinet. Mech. Cat.*, 2015, 114 (2): 753-766

[44] Pan H, Zhang YW, Shenoy VB. Effects of H-, N-, and (H, N)-Doping on the Photocatalytic Activity of TiO_2[J]. *J. Phys. Chem. C*, 2011, 115 (24): 12 224-12 231

[45] Asahi R, Morikawa T, Ohwaki T. Visible-Light Photocatalysis in Nitrogen-Doped Titanium Oxides[J]. *Science*, 2001, 293 (5528): 269-271